Department of Geophysics
Stanford University
Stanford, California

MICROBAROGRAPH STUDIES III

by

Jon F. Claerbout and Lee Lu

Final Report
Dec. 30, 1971

Work Sponsored by Advanced Research Projects Agency
ARPA Order No. 1362-69

Project Code No.:	9F20
Date of Contract:	1 April 1969
Contract No.:	F44620-69-C-0073
Contract Termination Date:	31 August 1971
Project Scientist:	Jon F. Claerbout tel. (415) 321-2300 x 3717
Short title of Work:	Telebaroms at LASA

This research was supported by the
Geophysics Division, AFOSR,

39

TABLE OF CONTENTS

I. Forward

This is the final report of the atmospheric wave studies project at the Stanford Geophysics Department. We have produced two previous reports (Microbarograph Studies, May 1970, and Microbarograph Studies II, March 1971). In this forward we will briefly review earlier results and in the main body of the report we will report the results of March to Sept. 1971. Despite the termination of this project we expect to continue to operate the 3 microbarographs for as long as possible and to work intermittently on interesting theoretical questions which have been raised. Our efforts have been in two principal directions: First we have been interested in computer modeling of global infrasonic waves. Second we have been interested in atmospheric turbulance, particularly the kind which interfers with the reception of infrasonic waves. Supporting these efforts is our own data collection network of three Stanford stations backed up by occasional use of the LASA microbarograph data.

On the first topic, computer modeling of global infrasonic waves, our viewpoint has been diametrically opposed to the principal theoretical work which preceded us during the 1960's (work of Pfeffer and Zarichney, Press and Harkrider, Pierce, Claerbout, etc.). Earlier work emphasized atmospheric inhomogeneity with depth, neglecting the lateral inhomogeneity of wind and weather, oceans and continents, equator and poles. Such work was marvelously successful near source but in our estimation the matching of theory with experiment at great distances left a lot to be desired. Although model parameters could

be adjusted to make a good fit to the data we thought the model itself to be inappropriate. This was shown most dramatically by the data of Wexler and Hass. The world wide meteorological data gathered after the October 30, 1961 Siberian Nuclear Explosion (I am not aware of any larger explosion before or since that one) exhibited a tremendous asymmetry developed by the resulting disturbance. A particular curiosity which we began to think about was propagation through the antipodes. Available theory predicts a focus at the antipodes but the observations were of a highly confused and apparently disorganized situation which reorganizes itself into a quasi-circular wave as it leaves the antipodes. We chose a suitable set of approximations which enabled us to compute the behavior of a monochromatic wave in the appropriate geometry with the appropriate material inhomogeneity. This is documented in our first report. Then in our second report we extended the computer modeling method from monochromatic waves to time dependent waves. In a later section of this report we show an example of the use of the method in a study on the development of "tails" or "codas" on propagating waves in inhomogeneous media. As far as atmospheric gravity waves are concerned there is still an important aspect of this modeling method which we were unable to complete for this report and on which we expect to continue to work. Our present method, although it encompasses the lateral inhomogeneity, does not encompass the depth inhomogeneity so it does not predict the observed frequency dispersion. We have made some progress on this. In simple terms the remaining task seems to be to factor the frequency-dependent, squared, phase velocity into two causal parts. We have

found some approximations but we have not yet been able to improve them to the desired accuracy.

Our second major endeavor on this project is the study of atmospheric turbulence. This part has been mainly observational. We have operated a weather satellite picture receiving station and have been comparing the weather and jet stream situation to some computed correlation functions of the microbarographic data. Our initial efforts were mainly just getting all of the equipment to run. Later we were able to do correlation studies with the microbarographs and determine apparent direction and speed. Then this was compared to high altitude weather maps, low altitude weather maps, and satellite photographs of cloud cover. Our final data analyses and conclusions are in this report. Also in this report are the last details in documentation of our electronics.

II. Results of Simulation of Air Waves in Atmospheric Lateral Inhomogeneity

Utilizing the theory developed in the last report we wrote a computer program to simulate the behavior of an acoustic wave propagating through atmospheric lateral inhomogeneity. Although the method works with a partial differential equation and it is possible to simulate a situation with a highly complex, realistic model we decided instead to run a simpler model in the hopes of isolating the important effects.

First we had to make the decision whether to model lateral variations in atmospheric temperature or in the wind. Since our data is most influenced by Pacific Ocean conditions we considered typical fluctuations of winds aloft to be of order $\pm$ 20 meters/sec and typical regional temperature fluctuations at a given altitude and time to be of order 5 decrees C. This amount of variation in winds causes about a 13% variation in sound speed but the temperature causes only about 1.5% sound speed variation (sound speed goes as the square root of absolute temperature). Thus we decided to model the effect on propagation of a global air wave caused by a circulating wind cell. A sketch of the geometry is in figure 1.

The travel time t_1 for propagation in the direction of circulation is given by

$$t_1 = \frac{d}{c + v} \approx \frac{d}{c}\left(1 - \frac{v}{c}\right) \qquad (1)$$

and the time for propagation against the circulation is

$$t_2 = \frac{d}{c - v} \approx \frac{d}{c}\left(1 + \frac{v}{c}\right) \qquad (2)$$

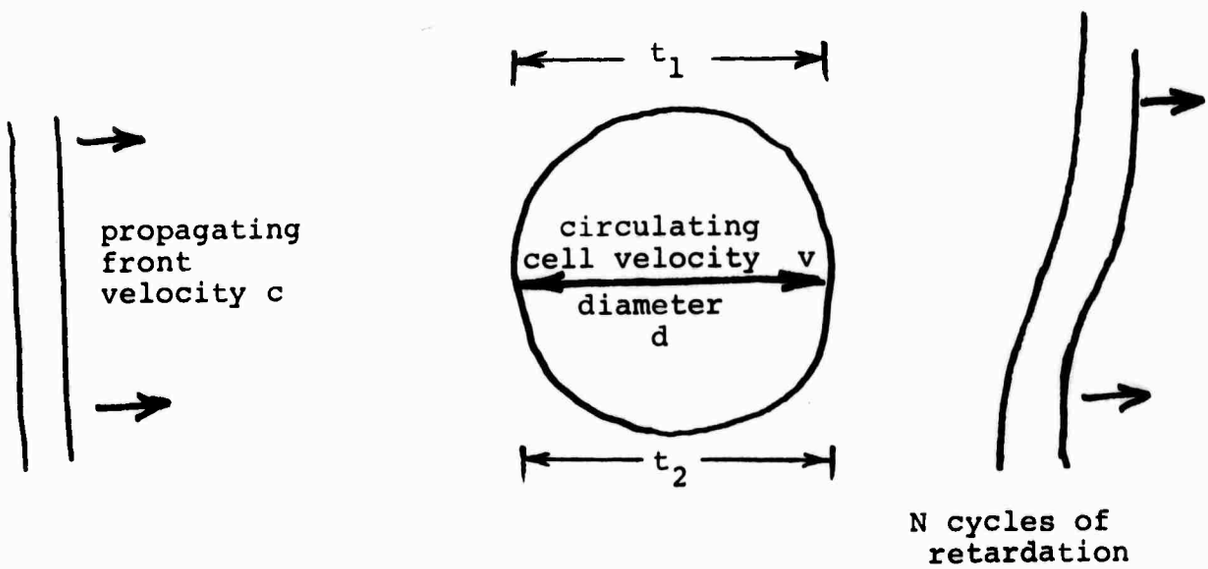

Figure 1. Geometry for phase advance and retardation of an atmospheric wave propagating through a circulating wind cell.

The number N of cycles of retardation of a quasi-periodic disturbance of period T (typically 6 minutes on a global propagation) may be set equal the differential travel time.

$$N\,T = t_2 - t_1 \quad \text{sec}$$

$$= 2dv/c^2 \quad \text{sec} \tag{3}$$

Taking a wind speed of $\pm$ 20 m/sec, a sound speed of 300 m/sec, a cell size of 400 km, and a wave period of 6 minutes we have

$$N = \frac{2 \cdot 400 \cdot 1000 \cdot 20}{6 \cdot 60 \cdot 300 \cdot 300} = \frac{1}{2} \text{ cycle} \tag{4}$$

Thus we anticipate that even under very modest conditions 180 degree phase shifts or sign reversals may easily occur in global propagations due to circulating wind cells.

Now for the purposes of numerical simulation we will take N fixed at 1/2 cycle. Since the sound speed is 300 this means that the simulation results will be applicable to values of

$$\frac{dV}{T} = \frac{Nc^2}{2} = 20{,}000 \quad (\text{m/s})^2 \tag{5}$$

For example, a 1.5 minute period wave could correspond to a 200 km cell at a 10 m/sec rotation rate.

Next we faced the problem of cell geometry. Perhaps we should have studied the disturbing effect of a single weather cell. Instead what we did is arrange a periodic structure of cells in a line as shown in figure 2.

Surprisingly it is after the wave has propagated through the air cells and while it is propagating in a homogeneous medium that

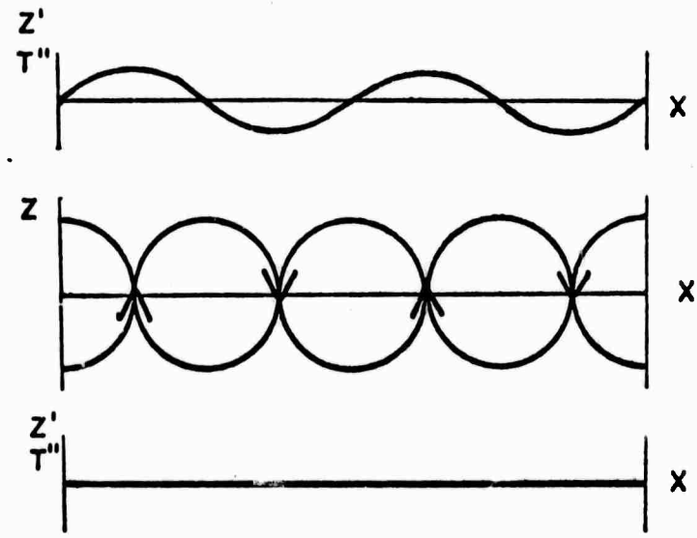

Figure 2. Possible means of producing a disturbed plane wave. Incident plane wave at bottom is altered by a material inhomogeneity (center) resulting in the disturbed wave at the top.

the principal disruption of the waveform takes place. The situation is depicted in figure 3.

The seven frames in figure 3 illustrate the subsequent development of the disturbed wave shown in frame #1. Note the frames may be thought of interchangeably in either steps of $\Delta t'$ or $\Delta z''$ as has been discussed in the previous report. The most obvious development is that the energy spreads out as one moves down the figure. The single pulse of the top frame has become an extended oscillatory arrival by the last frame. As time goes on less and less energy is in the first pulse and more and more is in the oscillatory tail. Note: in the figure the gain is adjusted with each frame to give better contrast. Also, as might be expected, the wave onset time, which is a dramatic function of x in the first frame, is really independent of x by the last frame. A surprising feature is that although energy moves back from the first arrival (see figures 1 and 2) a point of constant phase in the wave tail moves forward toward the first arrival (a point of constant phase is depicted with an X on the right side of each frame). Another clear feature of the wave tails is that dip (arrival time dependence on x) increases going down a single frame. The phase shift of the two dimensional focus, which causes doublets to form, is clearly visible in frame #2 marked with an A.

In order to represent a disturbance of infinite extent in x on a finite computer grid we initialized the problem with a periodic disturbance having zero slope at the side boundaries. Zero slope boundary conditions are then equivalent to infinite periodic extension in x.

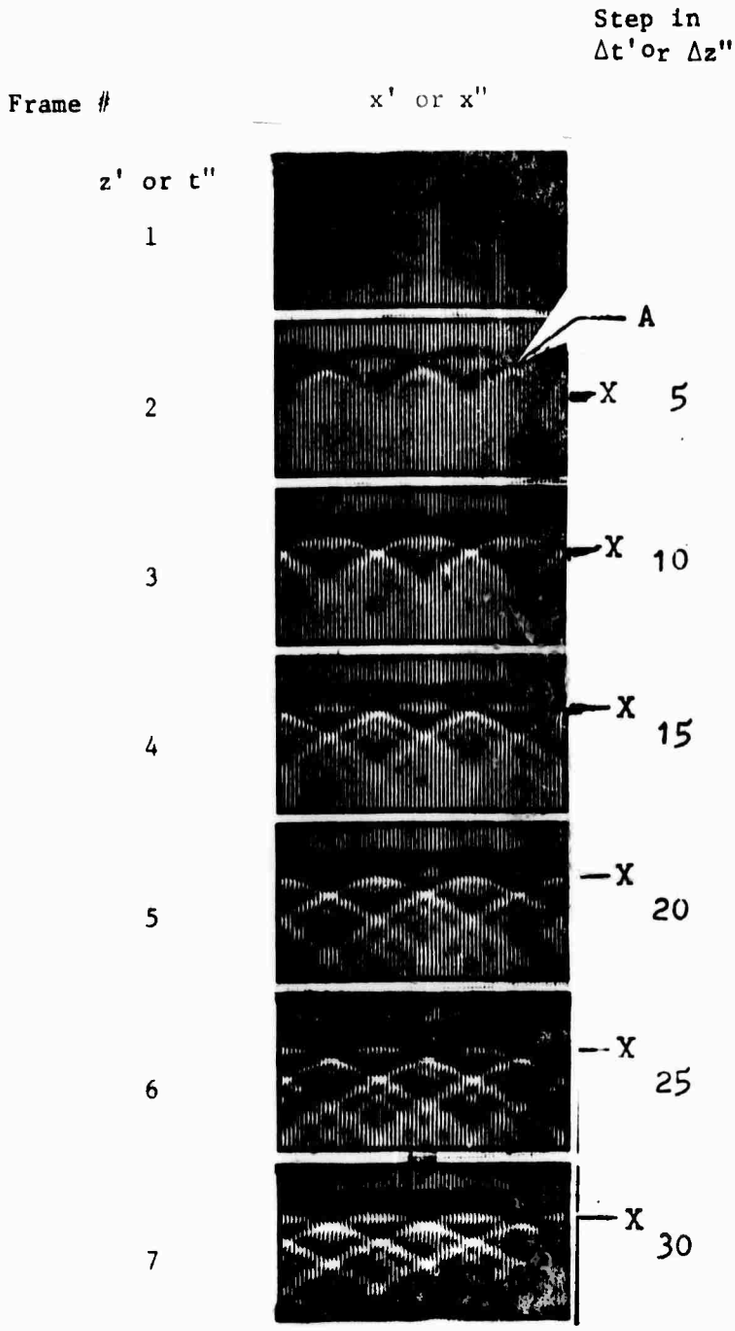

Figure 3. Disturbed plane wave propagating through a homogeneous region.

A value of a = 1/4 was chosen to give an appropriate variation in progressive frames with each frame in figure 4 representing 5 computational iterations. The solution may be rescaled in several ways due to the interdependence in the constant a (see equation 24) of $c\Delta t$, Δx and Δz. The calculation in figure 4 required about one half minute on the IBM 360/67.

It might be valuable to consider various data enhancement processes in the light of figure 4. In the process called "beam-steering" observations as in figure 4 would be summed over the x-coordinate in an effort to enhance signal and reject noise. Clearly beam-steering will enhance the first arrival while rejecting random noise. What it will also do is to tend to cancel signal energy which resides in the oscillatory wave tails. If one is really interested in enhancing signal to noise ratio it would hardly seem desireable to use a processing scheme which cancels signal energy. As z' or t" is increased the situation becomes increasingly severe since signal energy moves from the initial pulse toward the oscillatory wave tails. The central practical conclusion of this section is that what has often been regarded as "signal-generated-noise" may turn out to be signal in a potentially valuable form. We can, indeed, expect dramatic results if we are able to learn how to design data enhancement techniques on entire waveforms rather than on the initial pulse alone.

III. METEOROLOGICAL EFFECTS ON GROUND LEVEL PRESSURE FLUCTUATIONS

There has been growing interest in low frequency infrasonic theory and observaions during the past decade. Numerous investigators discovered that the jet stream may be the major source of energy input to both the lower and the upper atmosphere in the mesoscale range (Pinus et al., 1967; Claerbout, 1967). Tracking jet stream winds from ground level pressure signals in the east coast further confirmed this point of view (Herron et al., 1969). Using a linear model, Tolstoy et al. (1969) predicted the correct order of magnitude and power spectra for microbarographic fluctuations in the 5-60 min. range. To date, however, the generation mechanism and the source behavior of ground pressure fluctuations are still not fully understood. Further observation and data analysis are needed, especially in the area of prevailing jet streams.

In this section, the investigation of effects of large scale meteorological phenomema on the ground level pressure observations will be pursued. The jet stream winds were tracked from the ground level pressure fluctuations observed in Palo Alto area, in order to reconform the theory developed by Herron et al. and Claerbout. The data sampling rate and the frequency response of the digital data system made it possible to study pressure fluctuations ranging from 1.3 to 60 minutes.

(1) Jet stream and weather front activities

It is well known that belts of unusually strong westerly winds, the jet streams, exist near the tropopause region. Weather maps obtained from the ALDEN facimile recorder, which was connected to the FOFAX circuit network of the Weather Bureau, provided a valuable tool to locate the jet stream and the weather front activities. During the period of January through May 1971, cores of jet streams were found at altitudes in 200 mb, 300 mb, and 500 mb levels, ranging from 25 to 60 deg. north along the west coast of the U. S. and Canada. Fig. 4. shows time variation of latitude of jet streams and weather fronts at our longitude for 6 months.

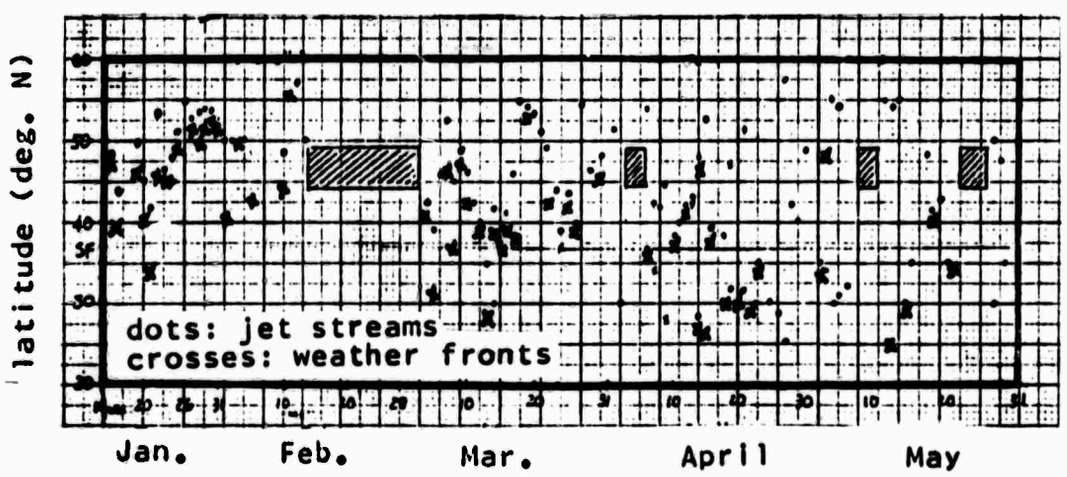

Fig. 4. Latitude variations of jet streams and weather fronts along the west coast of the U. S. and Canada. (The cross-hatched areas indicate sections of missing weather data.)

In winter, the big cyclone-like low pressure center, usually located in the nearby Alaskan region, causes the jet stream to head towards the coast of Washington more than any other area, because the jet stream always exists along the periphery of the low pressure cell. However, this low pressure center occasionally moves towards the east or the southeast in the northeast Pacific. The jet stream is then pushed forward, moving the weather front southward. Due to the passage of cold fronts and the effects of approaching jets, the local pressure field then becomes more prominent in high amplitudes and low frequencies. The cold front moves a short distance ahead of the jet streams, since the strongest winds are found along the cold side of the front zone. There exist both low and high altitude clouds linked with the jets as well as the front. This unusually dense cloud system can be quickly detected in satellite cloud pictures. (See Fig. 5. The site of observation is labelled at (1). Note the low pressure center, located at (2), with two jet stream systems ((3) and (4)), along with the front indicated at (5). As this low pressure center slowly moved in a southeast direction, the weather front and jet streams swept across the array of sensors. Meanwhile, another low pressure cell was developing at 55^{o}N 172^{o}E which is labelled at (6).) The pressure record of these events is presented later in this section.

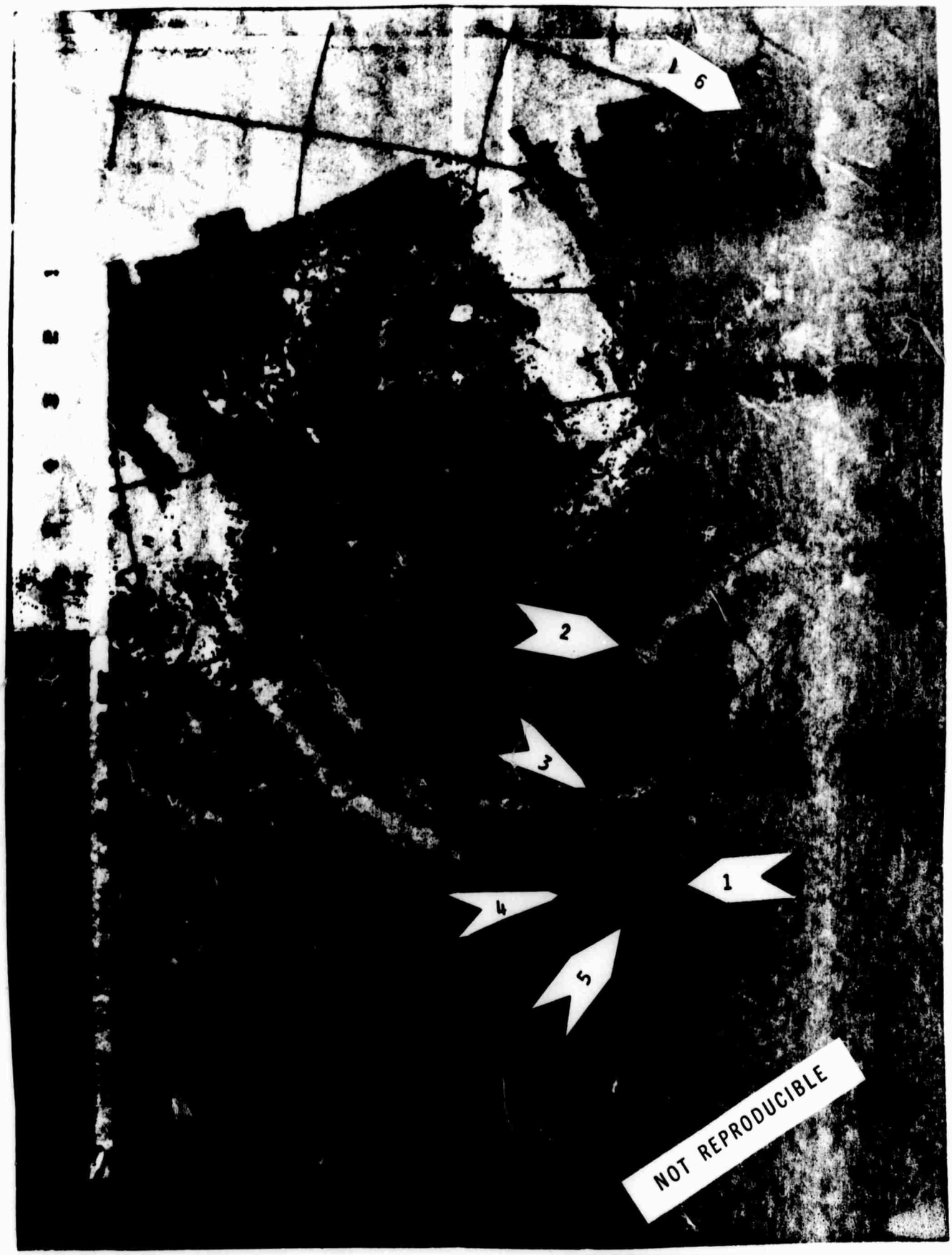

Fig. 5. The satellite mosaic cloud picture received at 8:00 PM April 6, 1971 showing the arrival of the weather front and the approaching of jet streams.

(2) Large-scale weather flow patterns in the northeastern Pacific region

Weather maps of 200 mb, 300 mb, 500mb, and satellite cloud pictures were collected daily from January through May 1971, to investigate the large-scale motions of the atmosphere which influence local pressure fluctuations. During the year, there were, in general, three types of large-scale flow which occurred in the area. They are discussed as follows.

(i) Flow Type A: This is the most common type of flow observed in the area (see Fig. 6a.). The three-dimensional, sinuous, jet streams are balanced by the pressure cells which tend to shift in various directions.

(ii) Flow Type B: In this type of flow, pressure cells are more stable and the low pressure cell has longer wave length (see Fig. 6b.). The direction of the ground pressure vector does not change as much as in Flow Type B.

(iii) Flow Type C: During summer daytime, the big low pressure center moves to the northwestern Pacific while the high pressure center takes the place of the low (see Fig. 6c.). Most significantly, the surface pressure fluctuations possess less energy. The local turbulence becomes relatively prominent and active.

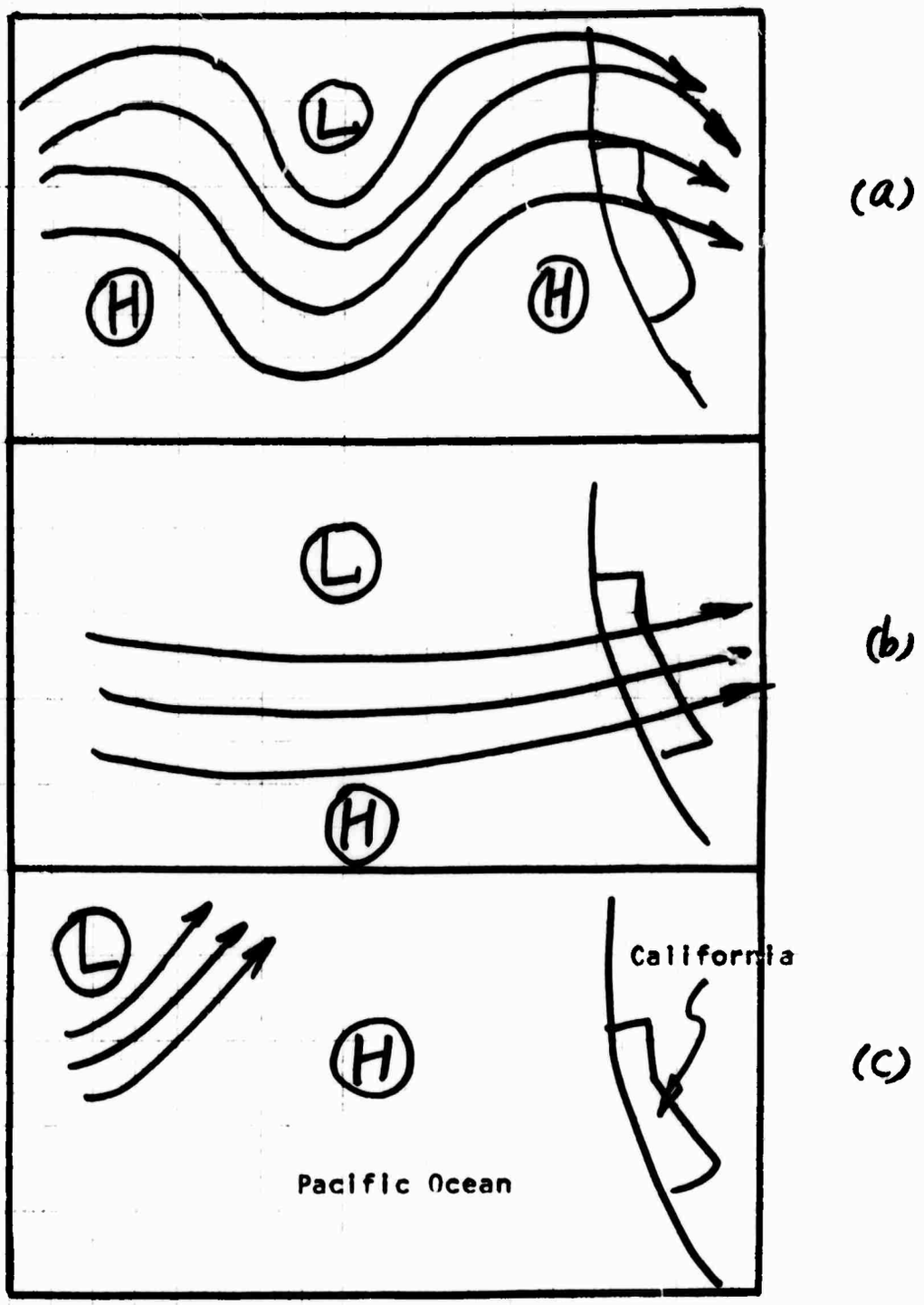

Fig. 6. Schematic diagram showing large scale flow patterns along the west coast of the U. S.

(3) Ground level pressure fluctuations

Ground level pressure fluctuations are recorded continuously, at a sampling interval of 40 seconds, from 5 km array of three microbarographs located in Palo Alto area. Three typical examples of the pressure fluctuations are described below:

(i) 5/9-11/71 (distant jet streams)
On 5/9/71, the high pressure center lay 400 miles offshore from San Francisco, while the jet streams flowed further north. This high pressure center moved slowly inland until it was over Washington by 5/11/71. Correlation of pressure waves with high altitude winds is difficult in this situation. The pressure records are given in Fig. 7.

(ii) 12/11-12/71 (nearby jet streams)
Fig. 8. shows the most coherent records we have ever recorded. The jet streams were very near, approaching from the northwest. Pressure fluctuations were greater in magnitude than usual. We believe that the impulsive arrivals on the pressure records are related to jet stream proximity but our weather data recorder was no longer in operation.

(iii) 4/5-6/71 (overhead jet streams)
The maximum in RMS pressure fluctuations on Fig. 9. at 2200, 4/5/71 is thought to relate to the weather front indicated by arrows numbered 4 and 5 on Fig. 5. A later RMS pressure fluctuation maximum at 900, 4/6/71 is thought to relate to the jet stream inducated by the arrow at 3.

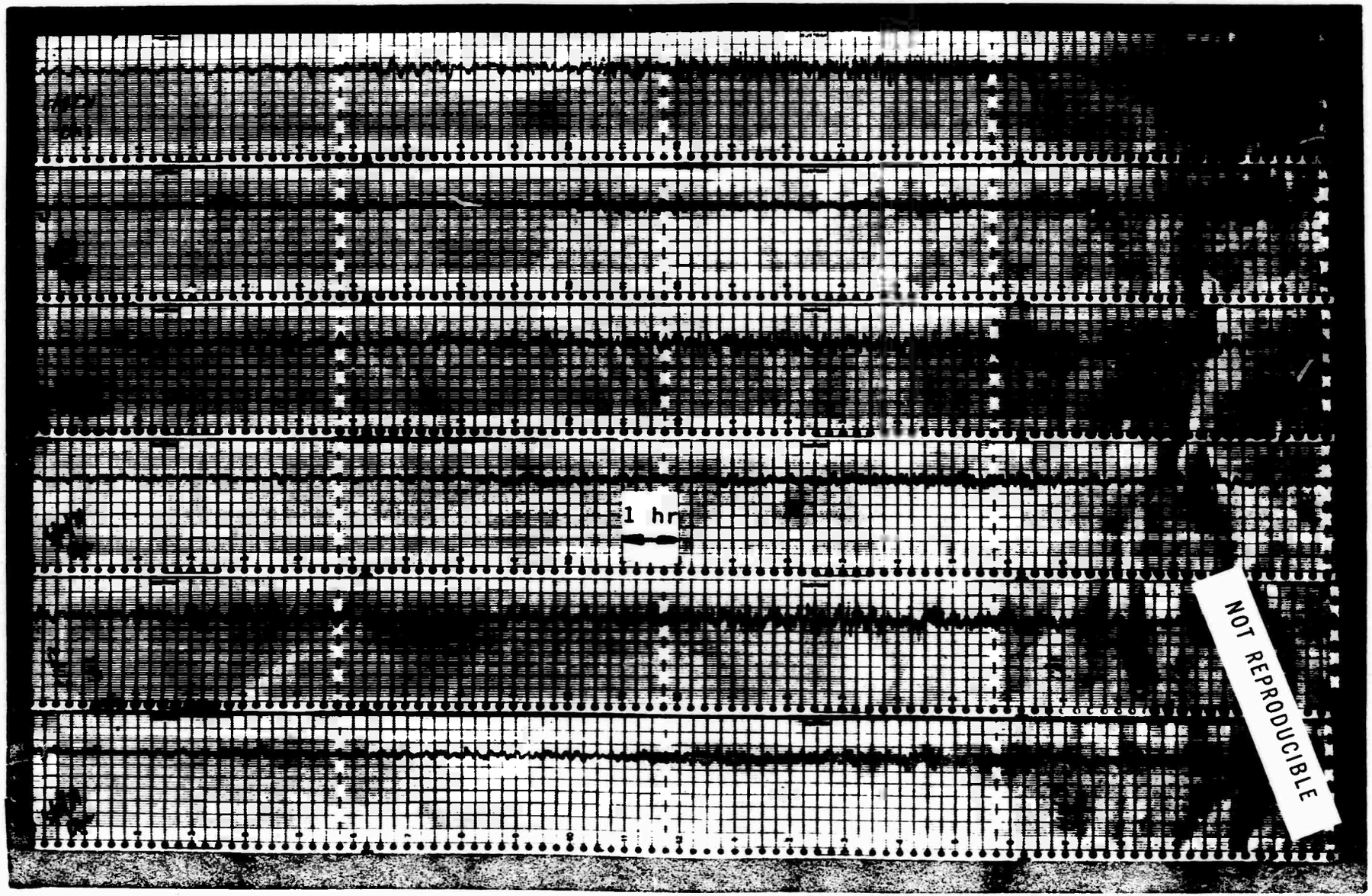

Fig. 7. Three days (5/9-11/71) of pressure fluctuations at two points (CH 2 and CH 3) seperated by 5 km.

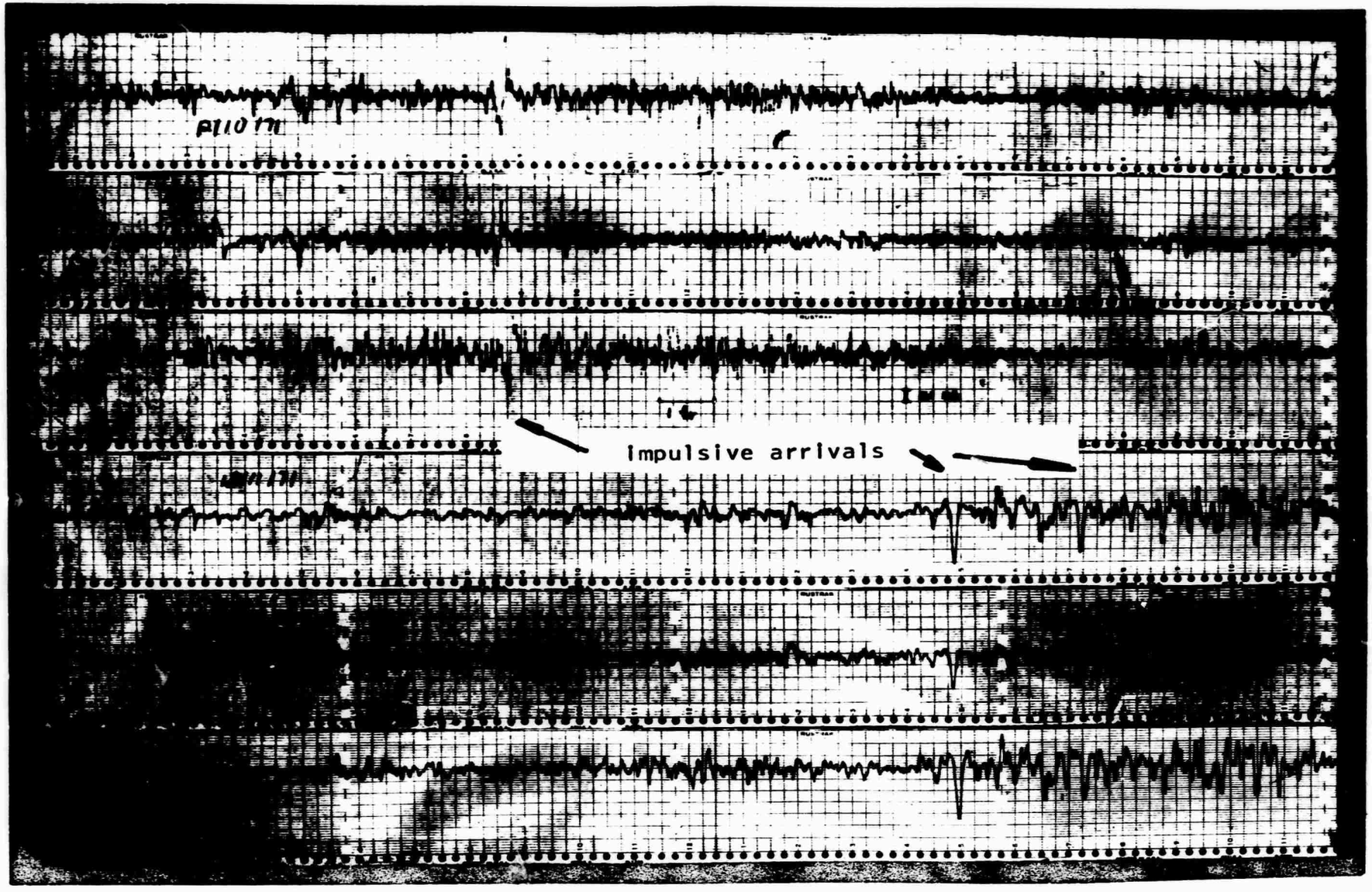

Fig. 8. Three-channel pressure fluctuations observed in December 10-11, 1971.

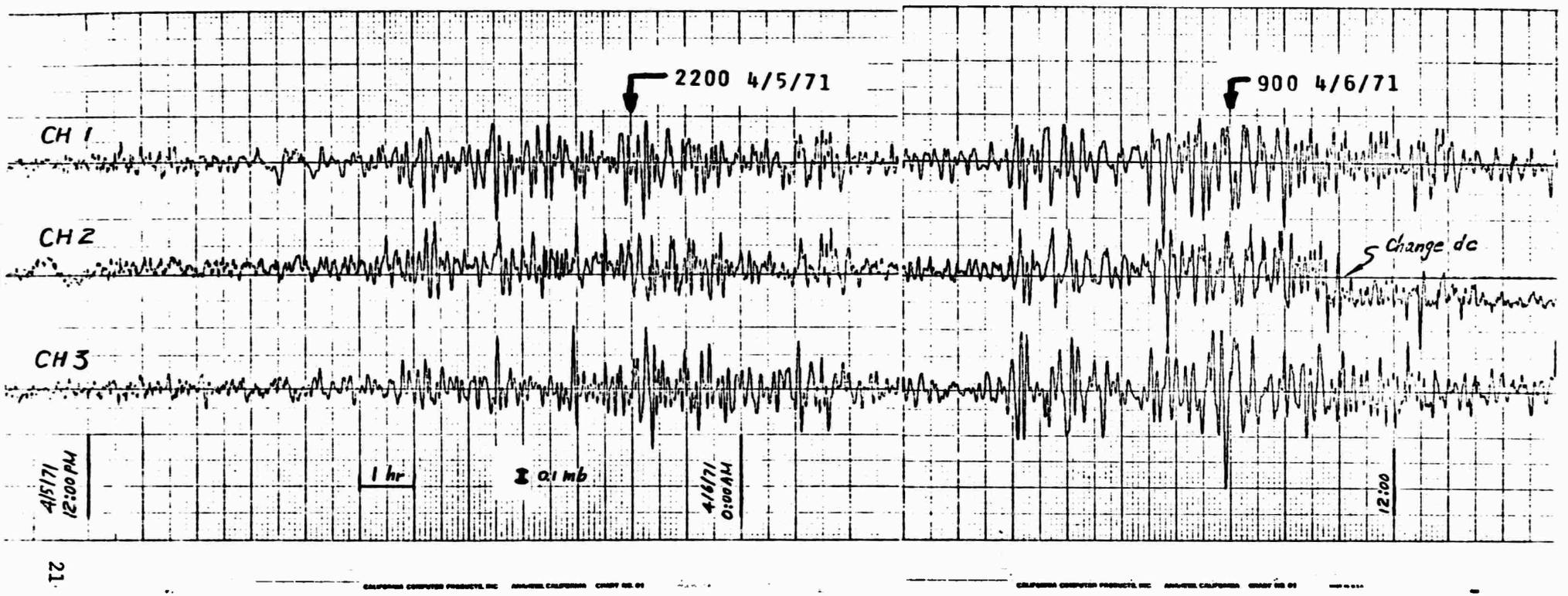

Fig. 9. The three-channel atmospheric pressure fluctuations observed during the weather front passage and jet stream activities in 4/5-6/71, plotted by the Calcomp plotter using data stored on the 7-track magnetic tape.

(4) Ground level pressure fluctuations generated by the cold air-mass

On 9/12/71, a strong, warm, high pressure ridge covered most of the western U. S. and parts of the Pacific Ocean. This aloft high pressure center lay over the state of Nevada. At the surface, meanwhile, the ridge of high pressure extended eastward from the coast into the northwest states. This would cause fair, hot weather over the state of California, along with a very quiet pressure field that was detected by pressure measurements in Palo Alto area (The pressure records are shown in Fig. 10.). On the next day, the center of this high altitude pressure center shifted westward to a location about 600 miles west of San Francisco. A large high pressure area, lying on the surface, rested with its center 400 miles of the Washington coast. This caused a general westward flow through most of California to bring the warm, dry air from the interior to the coastline. The temperature at San Francisco airport was very hot at 101 deg. F. On the following day (9/14/71), the high pressure center shifted northward into the western Canada. Meanwhile, a small, low pressure center formed and began to move slowly northward along with the cold air-mass. The arrival of the pressure signal was clearly observed at 5:00 am 9/14/71 (also illustrated in Fig. 10.). The corresponding pressure fluctuations might be generated by the shear instability in the frontal zone of the cold air-mass. In next two days, a number of high amplitude signals were observed (see Fig. 11.). The most likely source of these signals was believed to be related to jet streams.

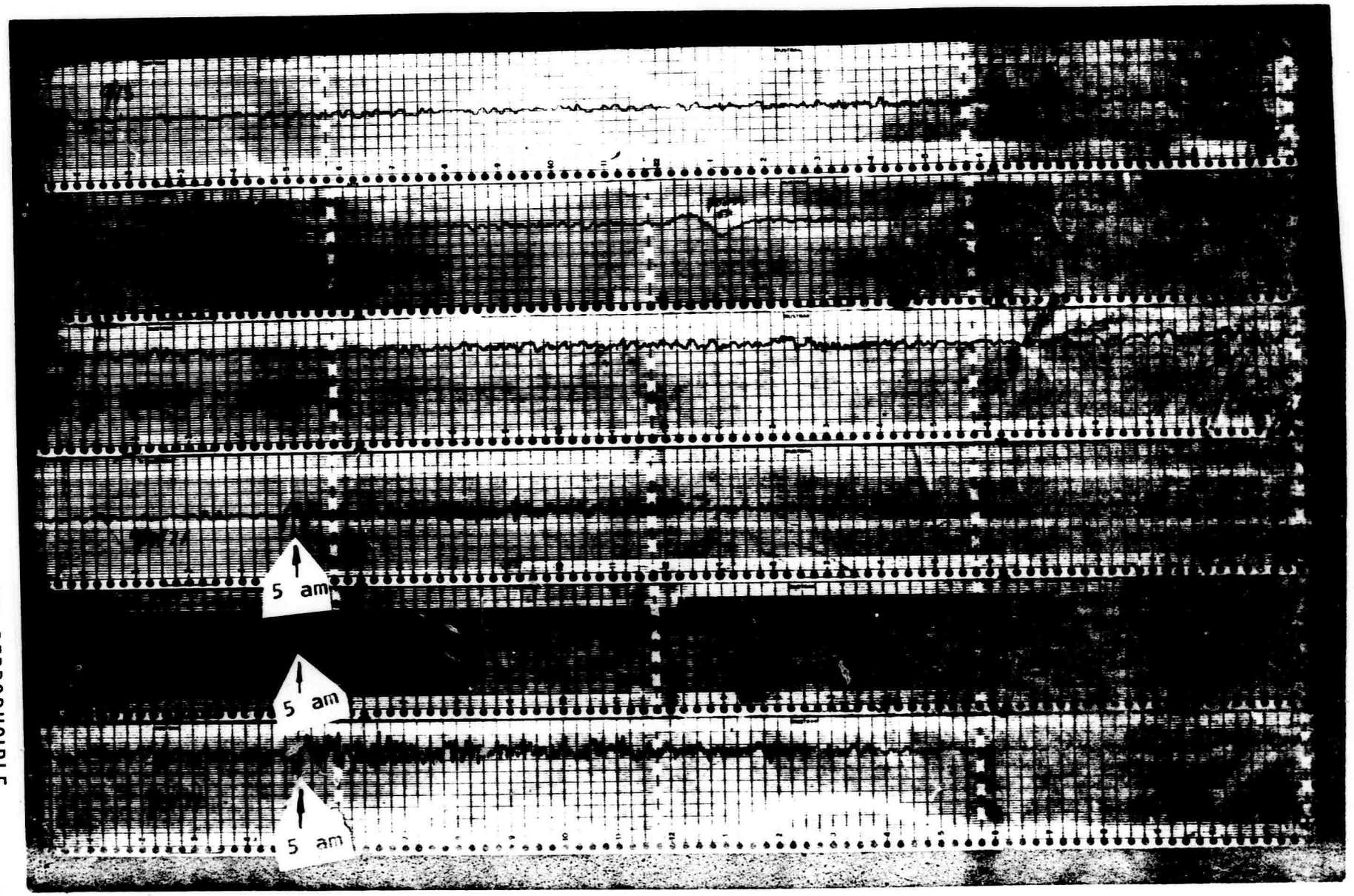

Fig. 10. Three-channel pressure records of 9/13-14/71. The cold air-mass arrived around 5:00 am, 9/14/71.

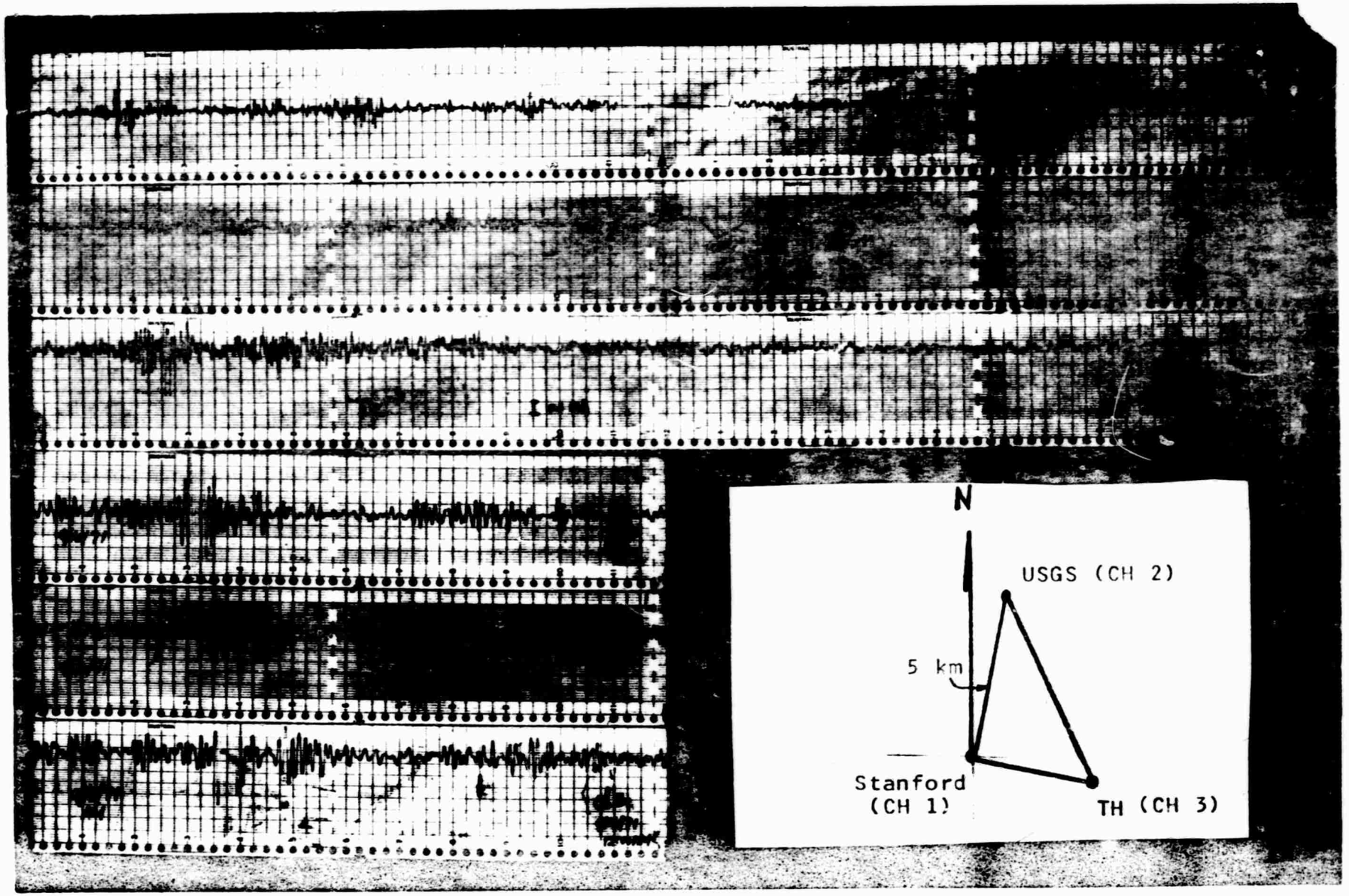

Fig. 12. Three channel pressure records (from 0000 9/15/71 to 1200 9/16/71) with the location of the stations. (Most of the pressure signals were from the southwest direction.)

IV. DATA ANALYSES

Infrasonic signals from all stations were recorded and processed. The previous report described the 5 km triangular array of three microbarographs, the tape format of the digital data system, and computer programs. In this section, the influence of large-scale weather on atmospheric pressure power spectra and the velocity of ground level pressure fluctuations will be analyzed.

(1) Power spectra

Samples of power spectra from the data of 3/5/71 and 4/6/71 were computed. They represented overhead and nearby jet streams respectively. In the case of nearby jet streams (see Fig.13a.), the spectrum showed large amplitudes in very low frequencies (larger than 35 min. in period) and the prominent high frequencies of periods less than 1 minute (Fig.13b.). Conversely, in the case of overhead jet streams, the large amplitudes were concentrated in the band-pass of periods in 1 to 8.5 min. This constrast might be explained by the influence of large-scale turbulent cells generated by the shear instibility of high altitude winds. When jet streams were overhead, the cells were stronger in strength and the ground-level pressure fluctuations had most of the energy in 4 to 35 min. period range. When jet streams were at distance away, the size and the strength of large-scale turbulence became larger and weaker as the small-scale turbulent cells developed rapidly. Thus, part of the energy shifted to

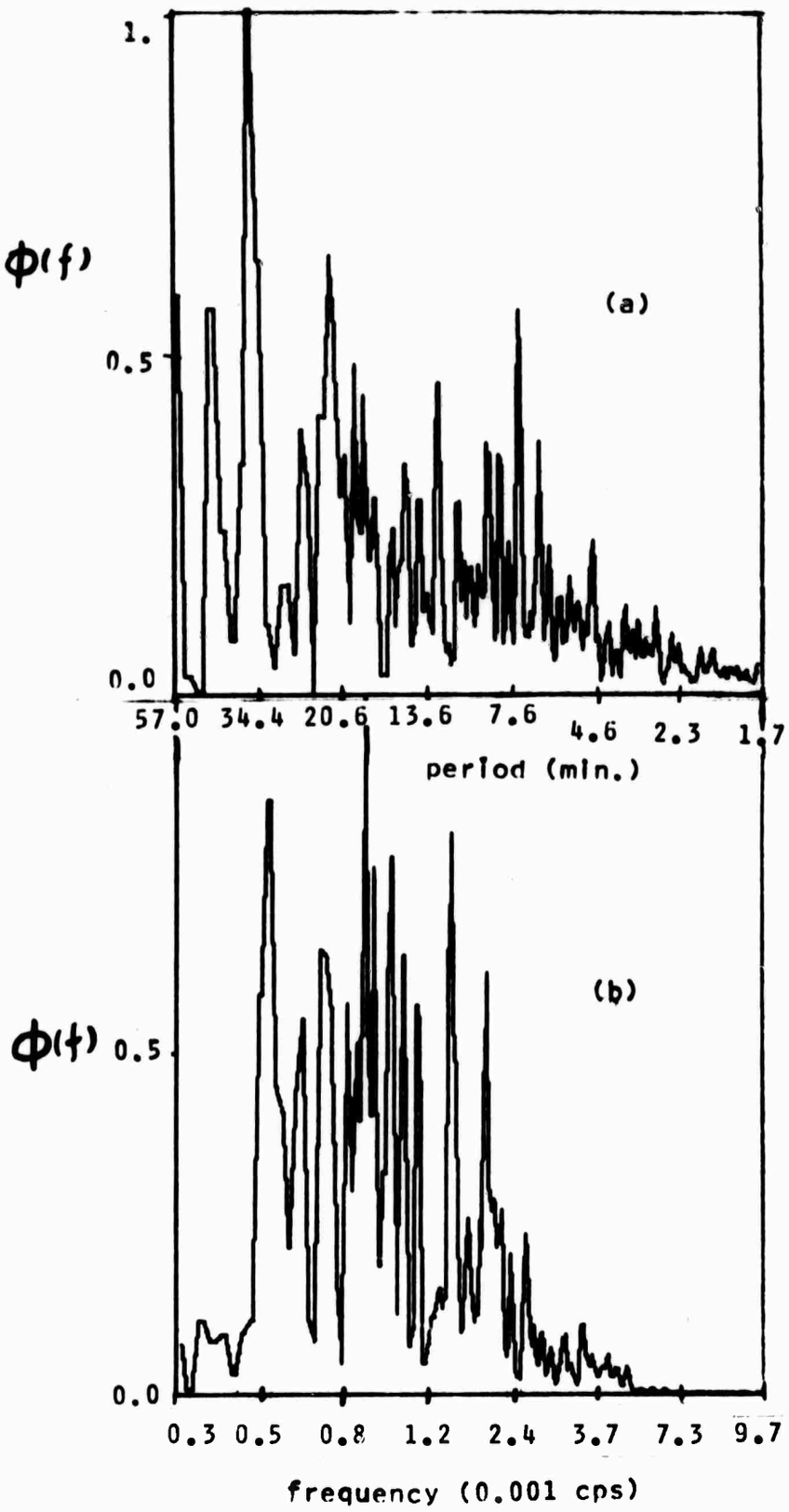

Fig.13. The atmospheric pressure power spectra for Channel 3.

(a) 8-hr of data from 3/5/71 (nearby jet streams).
(b) 8-hr of data from 4/6/71 (overhead jet streams).

higher and lower frequencies. A sample of the mean spectrum was also computed as shown in Fig. 14. The mean spectrum averaged out the fine structure of the individual time-dependent spectra, and represented the energy received during the period of averaging. Both the component spectra and the mean spectrum showed that jet streams were the major source of energy affecting the ground pressure fluctuations.

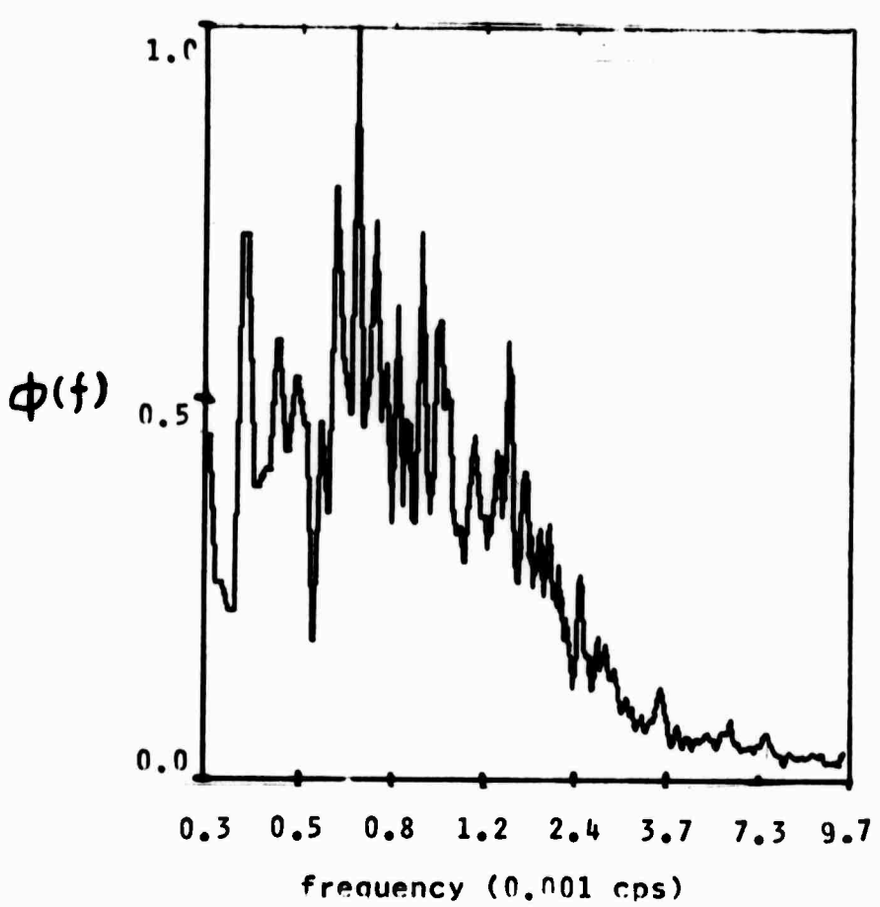

Fig.14. The mean atmospheric pressure power spectrum for Channel 3. (from 11 individual spectra of 3/4-14/71)

(2) Correlation of Ground-level pressure fluctuations with high altitude winds

The velocity vector of ground level fluctuations was calculated in order to correlate with high altitude winds. Instead of using a "running window" to look for the best coherent signals in the data, the "window" was fixed at 8 hours. This 8 hours of data were centered at 0:00 GMT, because the weather maps were available at that time. The correlation matrix matrix was then computed so as to give the coefficients of correlations for the three-channel pressure data. Of the three measured time lags on the correlations we selected the two most coherent in order to determine the apparent velocity. Though this is not an optimum procedure, a fairly consistant result was obtained. In Fig. 15., the components of 200 mb winds were compared to the components of ground level pressure fluctuations. The set of results on the left-hand side of the figure represents the flow type (a) discussed earlier in this report. The high-pressure cell moved overhead on 1/31/71 inducing both high altitude winds, and surface pressure waves, in a northwest direction. As soon as this high-pressure cell shifted 500 miles from the coast, the direction of winds and pressure waves changed to the southeast. The set of results on the right-hand side of the figure corresponds to the flow type (b), which has waves and winds mostly from the west except for minor changes in the north-south direction.

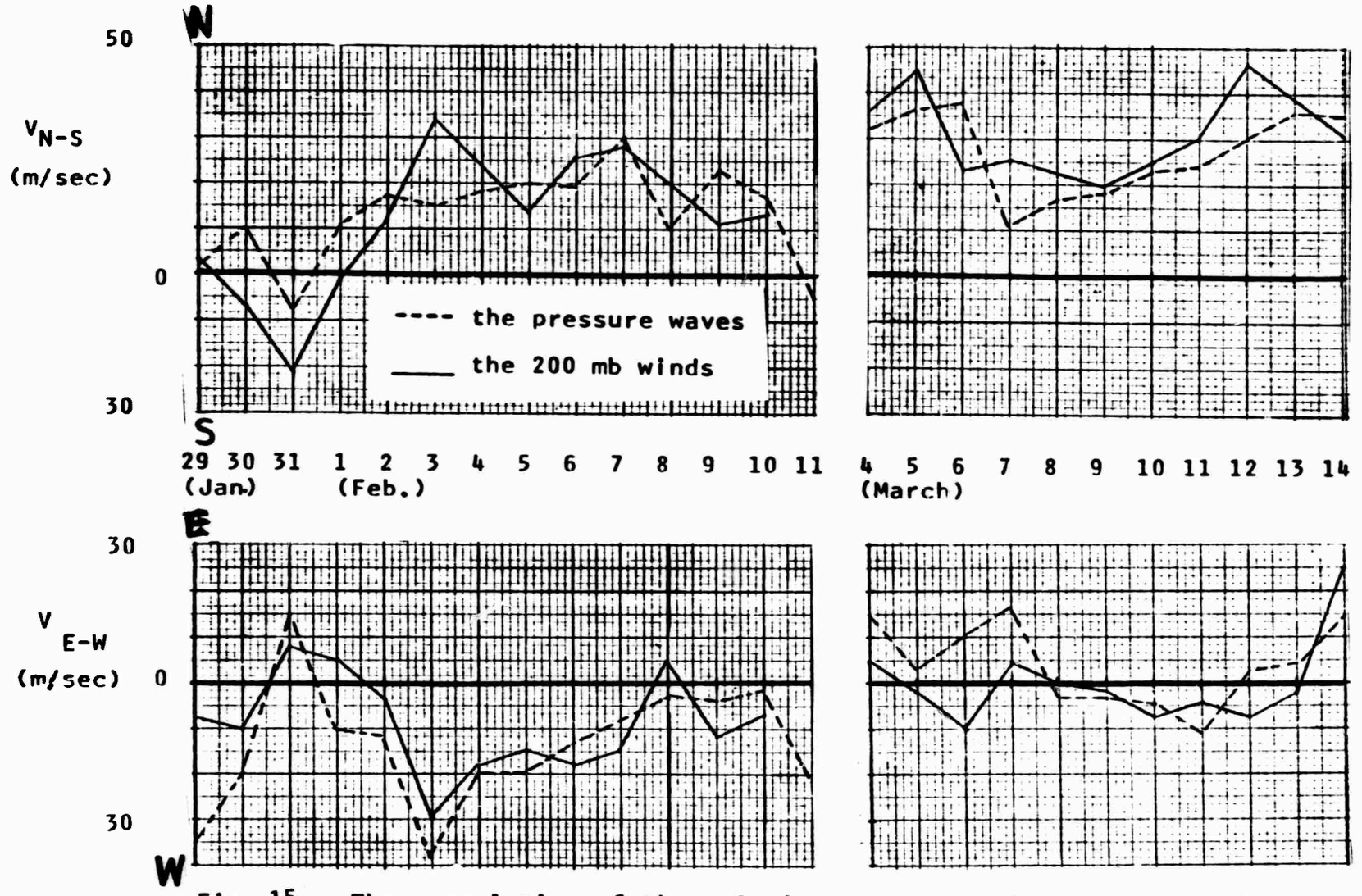

Fig. 15. The correlation of the velocity components between ground-level pressure waves, and 200 mb winds.

V. DISCUSSION AND CONCLUSIONS OF OBSERVATIONAL STUDIES

The frequent occurrences of jet streams, weather fronts and cold air-masses in Pacific northeast, the West Coast of the U. S. and Canada, provided the chance to study the effects of large-scale atmospheric motions on the local pressure field. Most conditions could be catagorized as one of three commonly occurring types of large-scale weather flow patterns. Correlation was observed between pressure wave strength, coherence and velocity with the weather flow patterns. This correlation raises the possibility of prediction of the local pressure field from the information gathered in large scale meteorological forecasting.

Occasionally overhead jet streams were recorded. They showed pressure fluctuations with amplitudes on the order of 1 mb, and frequencies in the period range of 1 to 10 minutes. The spectra of pressure waves showed that there was considerable energy input to the ground from jet streams. The weather fronts were found, usually, to be linked to the jet streams. Waveforms of both jet streams and weather fronts were similar enough in frequencies and amplitudes, to be hardly distinguishable. An exceptional case was the cold air-mass observed from south described earlier.

Ground level pressure fluctuations correlated reasonably well with

tropopause winds in periods ranging from 1.4 to 60 min. It is comparable to the results obtained from observations in Dobbs Ferry, N. Y. by Herron et al. Further observation of the wind velocity at each station should enable understanding of the importance of the effects of the boundary layer, the topography, and the structure of high frequency atmospheric turbulence.

In this study, satellite cloud pictures were used because jet stream activities could be easily detected from the dense cloud systems. We are making a movie from these pictures. This movie will show the possible jet stream locations, movements, and the corresponding responses of the ground pressure vector.

As a final note, the digital data acquisition system proved to be a versatile and economic system which required a minimum amount of maintainance and service. It is suitable for continuous low speed recordings of geophysical data.

VI. ACKNOWLEDGEMENT

This work was sponsored by the Advanced Research Projects Agency ARPA Order No. 1362-69. This support is gratefully acknowledged.

VII. REFERENCES

1. Claerbout, J. F., 1967; Electromagnetic effects of atmospheric gravity waves, Ph.D. thesis, M. I. T.

2. Herron, T. J., and I. Tolstoy, 1969; Tracking jet stream winds from ground level pressure signals., J. Atmos. Sciences, 26, 266-269.

3. McDonald, J. A., and Herrin, E., December, 1970; Very long period waves associated with atmospheric disturbances., Final report SMU No. 80-36.

4. Tolstoy, I., and Herrin, T. J., 1969; A model for atmospheric pressure fluctuations in the mesoscale range., J. Atmos. Sci., 26, 270-273.

VIII. APPENDIX

The Digital Data Acquisition System of Stanford Infrasonic Waves Laboratory

The digital data acquisition system records multiple analog input of the microbarometric pressure data in digital format on an IBM compatible magnetic tape. The Honeywell digital modules (FA-320, DI-320, Dm-335, CH-460, CH461, CH-459, and CH-463) have been used for constructing the system. The physical layout of the system is shown in Fig. 1.

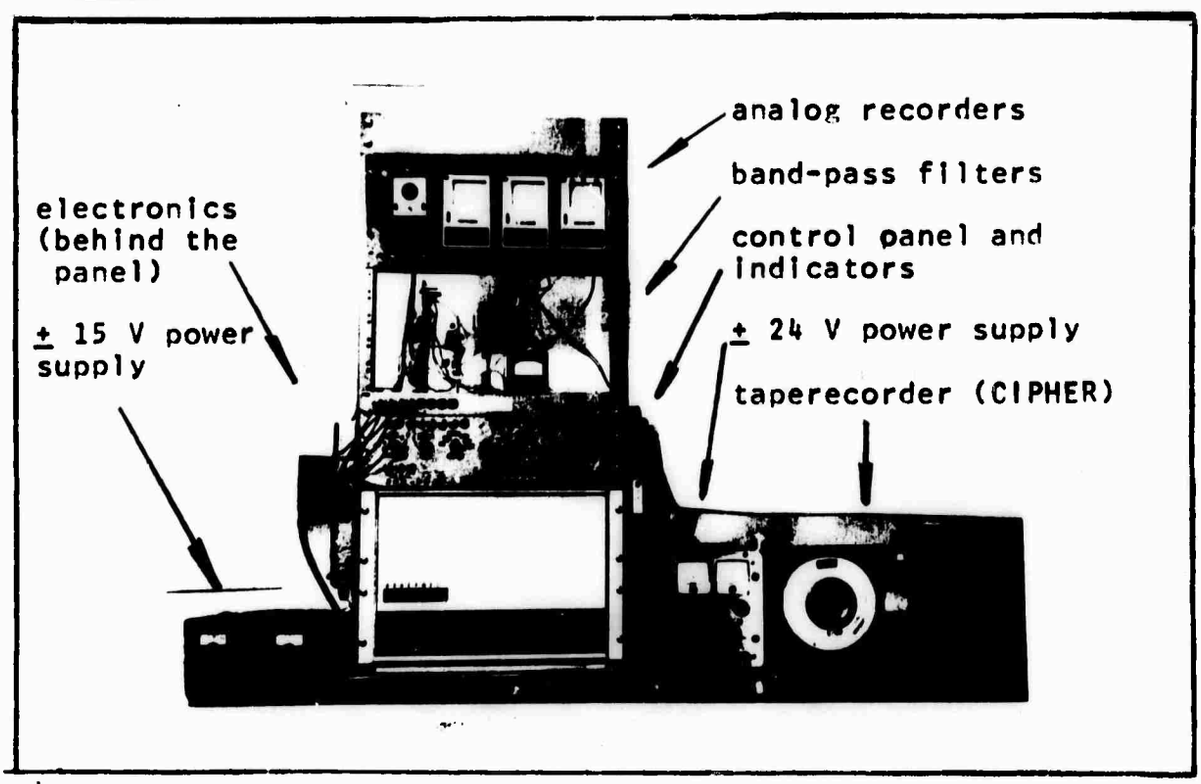

Fig. 1. The physical layout of the digital data system.

The theory of operation of the system is simple and straightforward. Timing functions are illustrated in Fig. 2. A 1 MHz clock (MC-335) is used as the basis of operation. The speed of the clock is divided into lower rates for purposes of low speed and continuous recording. The divided clock signals (c and $\bar{c}$) are then gated with the ON/OFF flip-flops and a NAND gate to give sampling functions which have rates ranging from 0.01 to 100 data/second. The writing speed is twice the sampling speed (because each word is written as two bytes), and the write command is then delayed by a Delay Multivibrator (DM-335) to trigger the multiplexer and the channel selection counter.

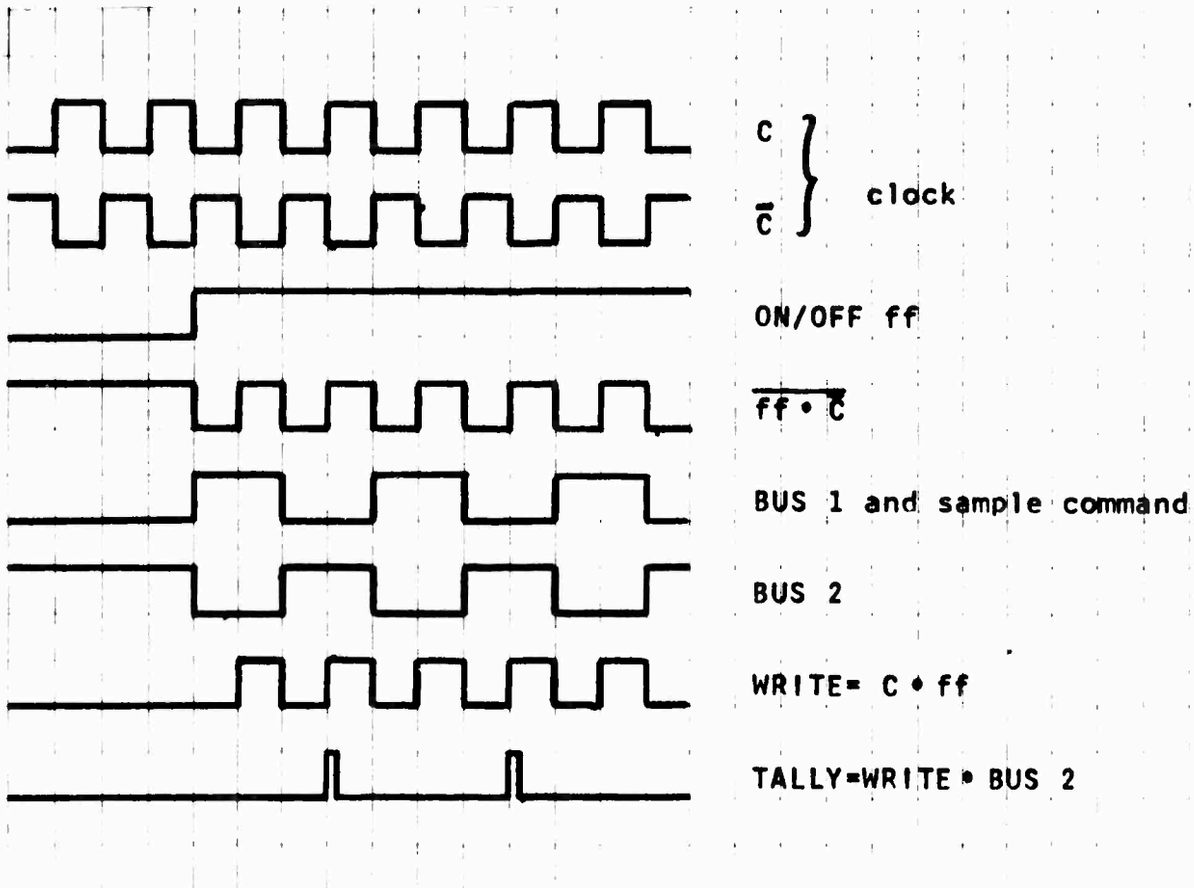

Fig. 2. Timing functions of the system.

The general specifications of the digital data system are listed as follows:

1. logical levels

   logical zero 0.0 V to 0.35 V (max)
   logical one 3.5 V to 6.30 V (max)

2. temperature range

   0 to 40 degrees C

3. Power supply requirements

(a) A/D	$\pm(24\pm1)$ V
(b) other circuits	$\pm(6\pm0.3)$ V
(c) lamp indicators	$+8\pm2$ V
(d) operational amplifiers	$\pm(15\pm0.5)$ V

4. current requirements

   They are listed in the specifications of each individual μ-PAC in reference 1.

5. accuracy of outputs

   The output accuracy of the digital sata system is approximately $\pm$ 0.15 V.

6. input requirements

   The input voltage of each channel should stay within +10 V.

The circuit diagram of the timing is illustrated in Fig. 3. This system samples 1 to 8 channels of data with the channel selection. The channel 8 has a special time-delay circuit (8CT) as shown in Fig. 8.. The channel selection counter (MUX) is presented in Fig. 4. The analog inputs first enter into the multiplexer (Fig. 5.) which selects channel by channel for A/D converter shown in Fig. 6. Then, it is stored in the 10-bits-word decimal form in the data matrix (Fig. 7.). The Fig. 9. indicates circuits of the multiple gaps counter (MCT) and the gaps control counter (GCT).

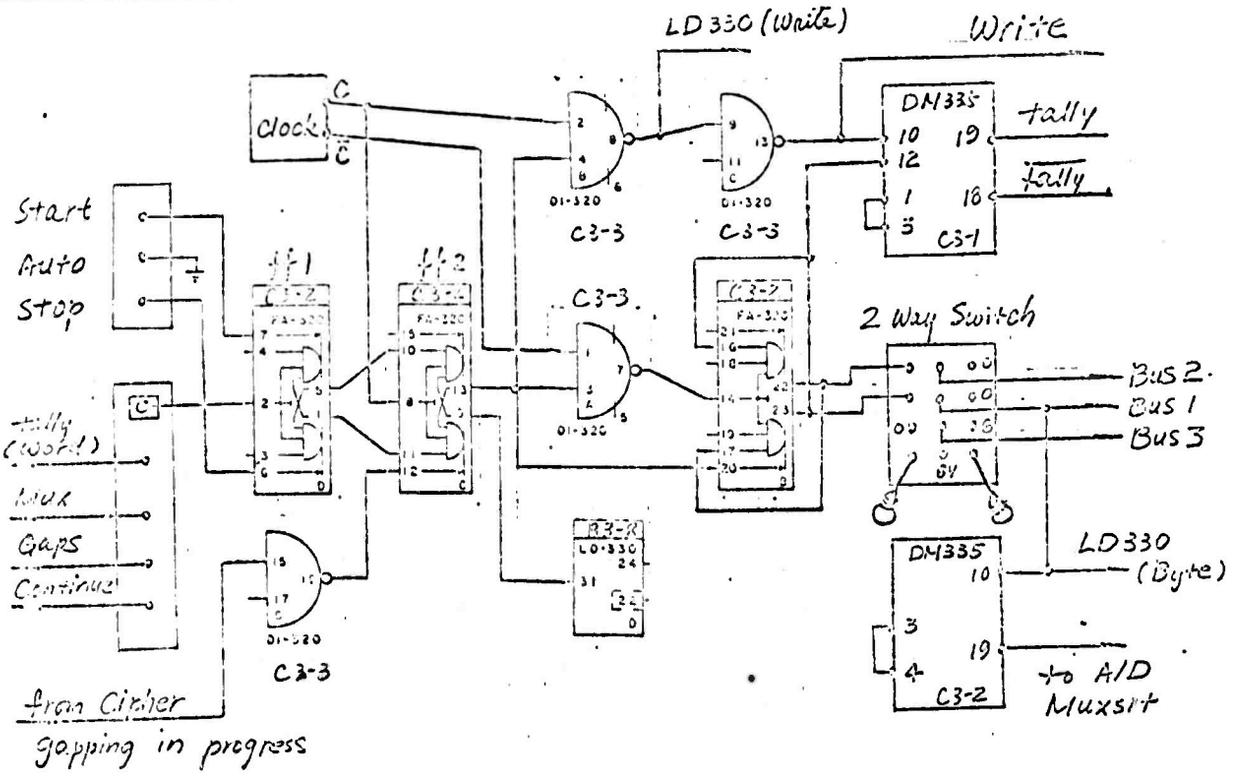

Fig. 3. Timing On/Off

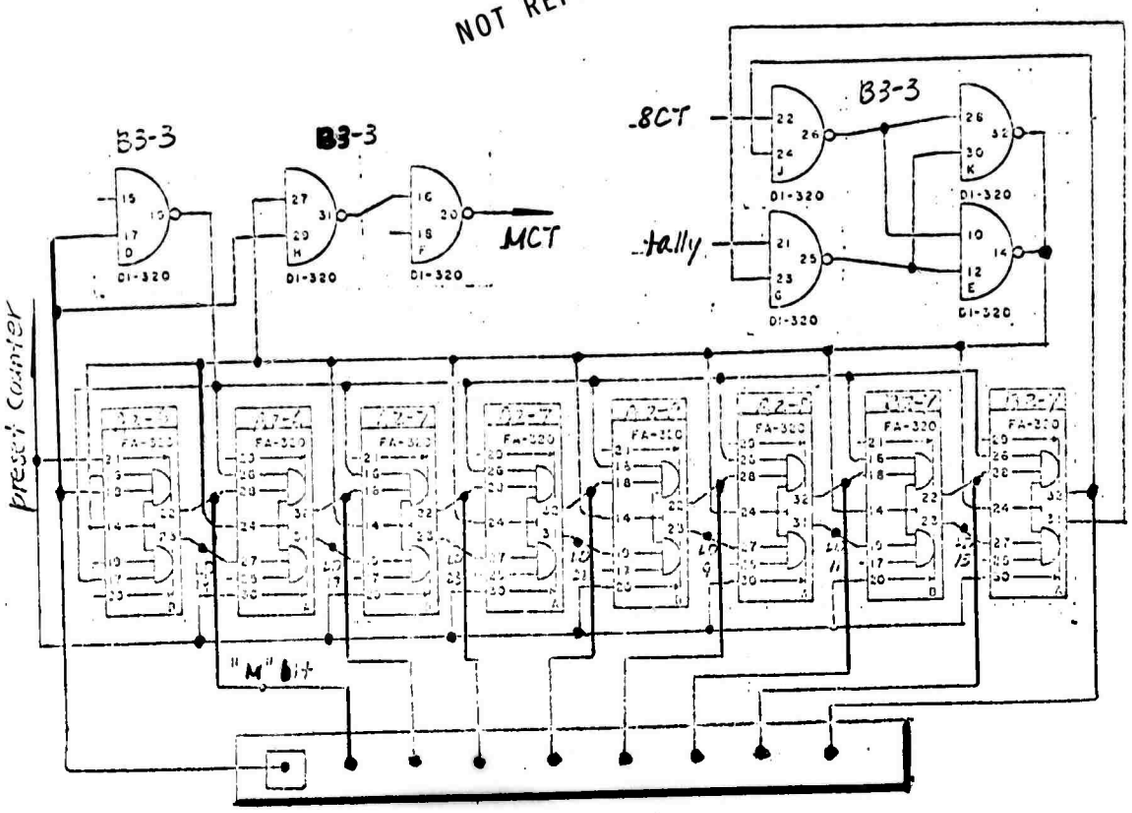

Fig. 4. MUX

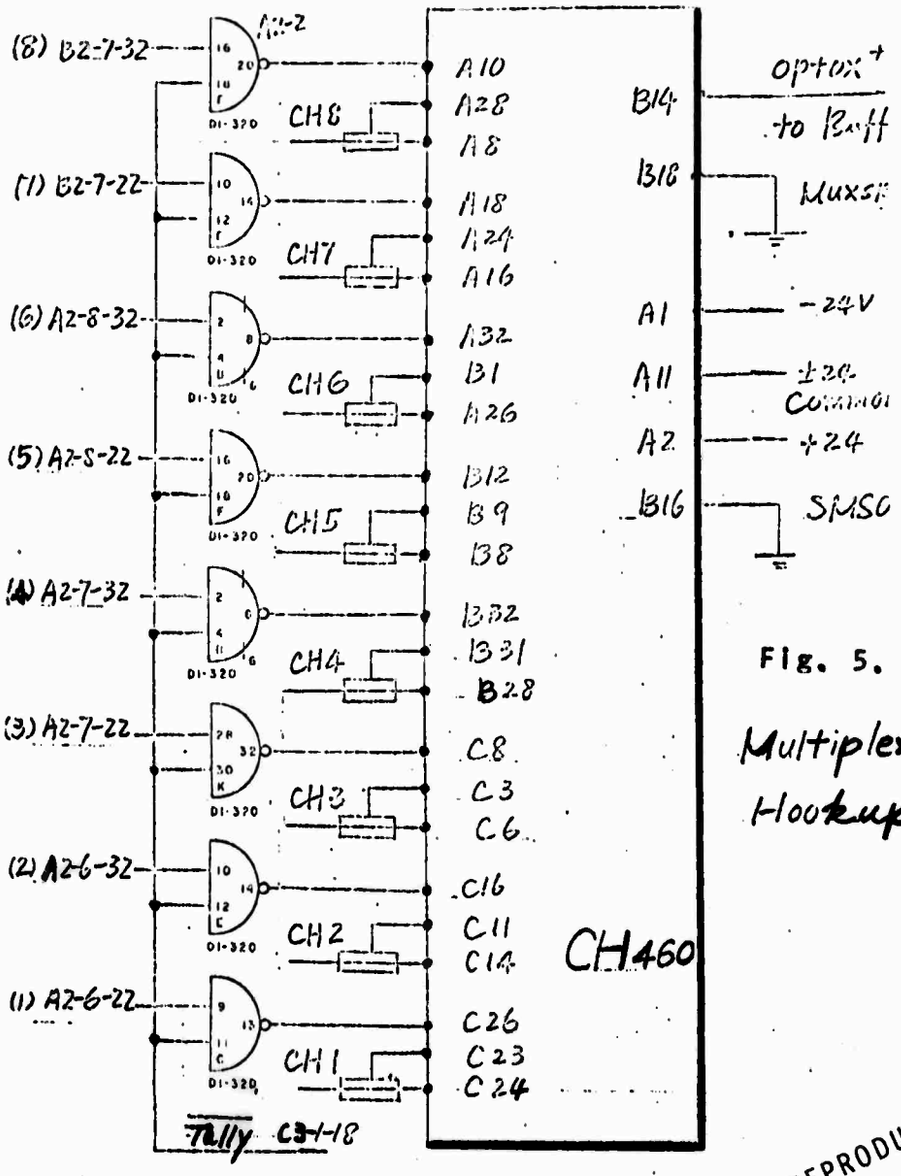

Fig. 5.

Multiplexer Hookup

NOT REPRODUCIBLE

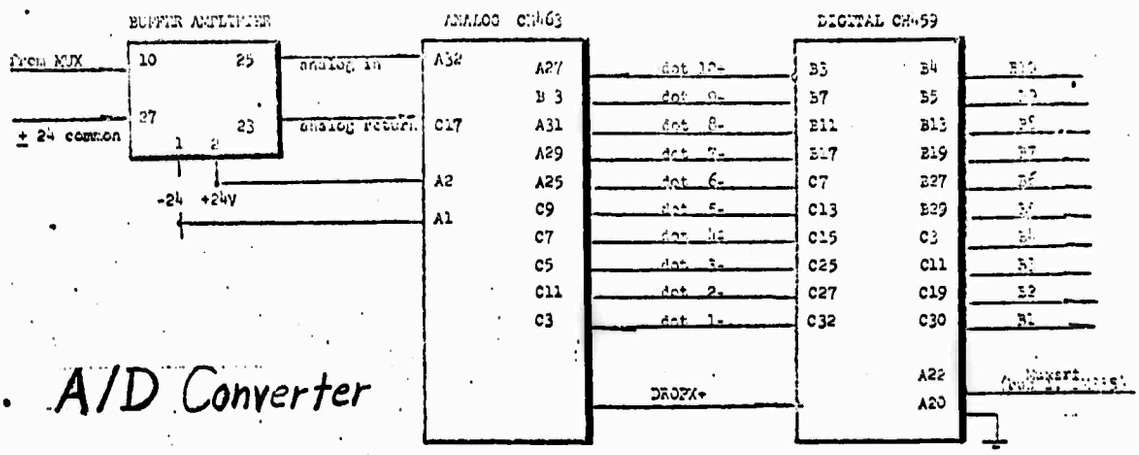

Fig. 6. A/D Converter

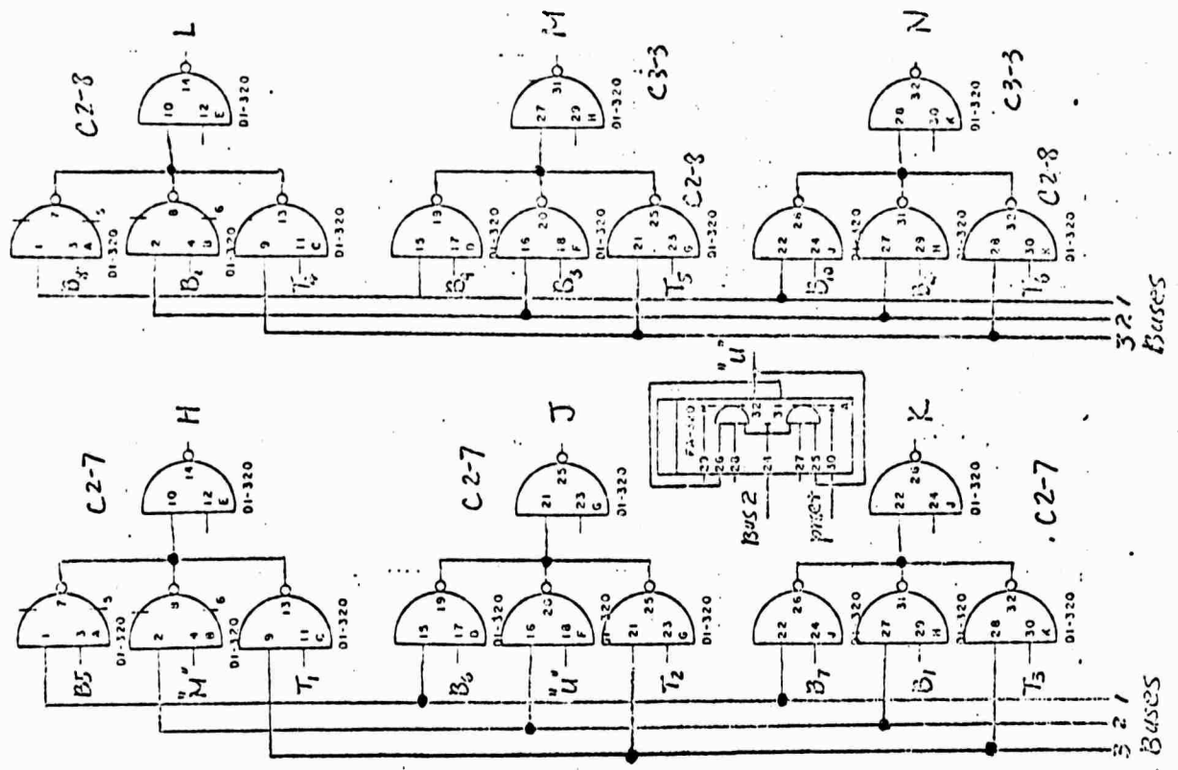

Fig. 7. DATA MATRIX

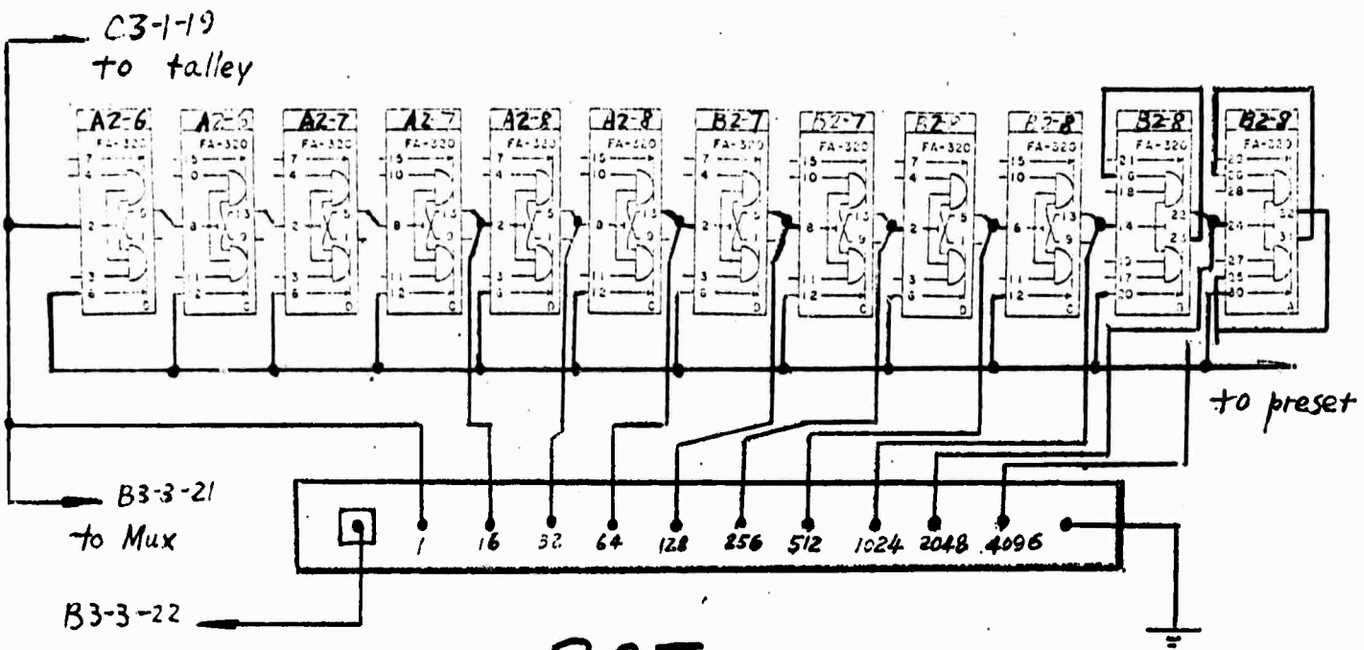

Fig. 8. 8CT

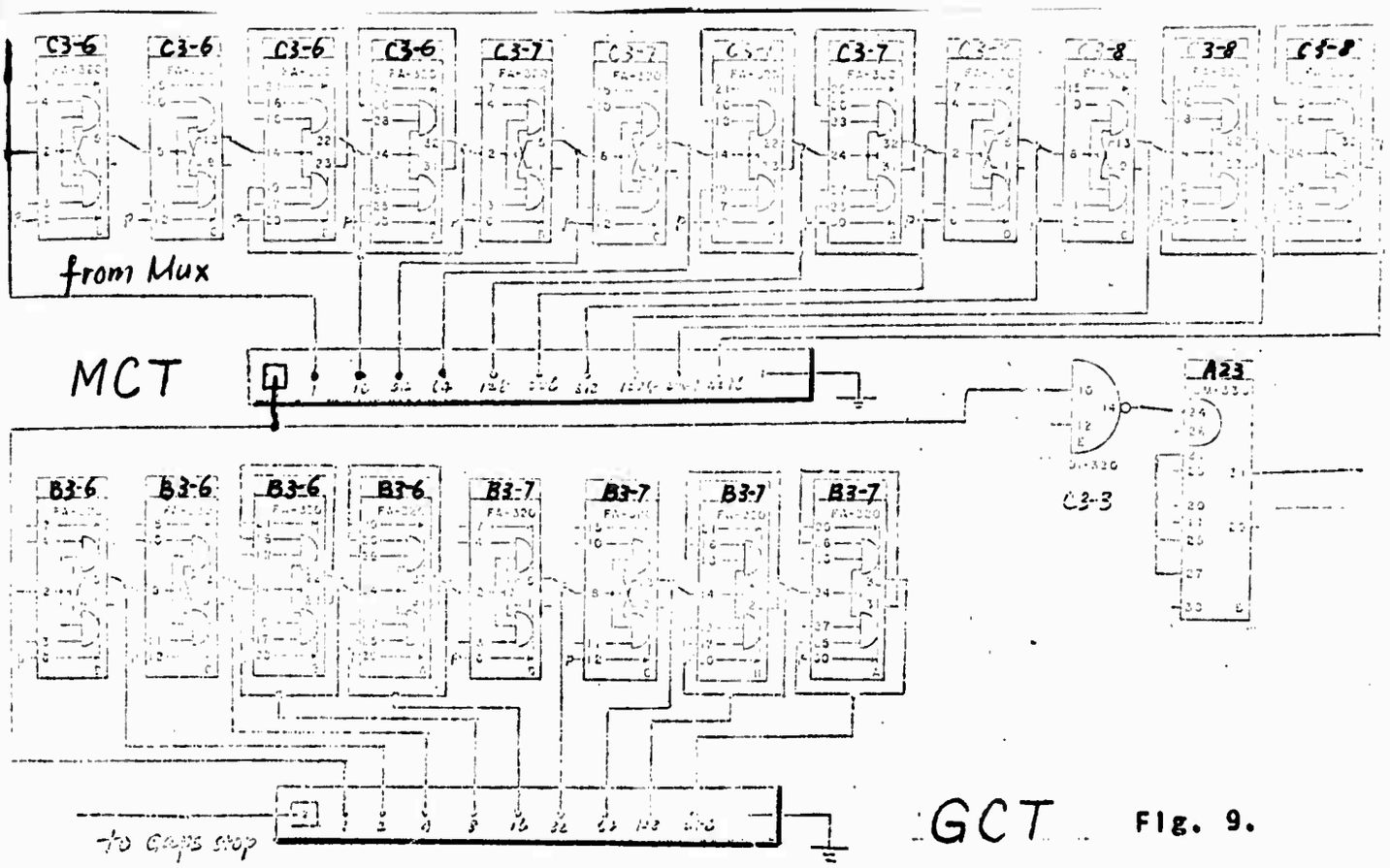

Fig. 9.

REFERENCES FOR THE APPENDIX:

1. Cipher Data Products, Inc.
Service manual, Model 70 magnetic tape recorder, 1968.

2. Honeywell Computer Control Division.
Instruction manual, μ-PAC Modules 5 MHz and 2 MHz,
Volume I and Volume II, 1968.

3. Lee lu and R. J. P. Lyon.
The Stanford Spectral Digital Data System,
Stanford RSL final report No. 71-3, 1971.

4. Montgomery Phister Jr.
Logical design of digital computers, 1968.